

# On the use of X-ray telescopes for identifying the origin of electrons and positrons observed by Fermi and PAMELA

Antoine Calvez\* and Warren Essey

*Department of Physics and Astronomy, University of California, Los Angeles, CA 90095-1547, USA*

Malcolm Fairbairn

*Physics Department, King's College, London, UK*

Alexander Kusenko

*Department of Physics and Astronomy, University of California, Los Angeles, CA 90095-1547, USA and  
IPMU, University of Tokyo, Kashiwa, Chiba 277-8568, Japan*

Michael Loewenstein

*Department of Astronomy, University of Maryland, College Park, MD, USA and  
CRESSST and X-ray Astrophysics Laboratory NASA/GSFC, Greenbelt, MD, USA*

Observations using X-ray telescopes can help understand the origin of the electron and positron signals reported by ATIC, PAMELA, PPB-BETS, and Fermi. It remains unclear whether the observed high-energy electrons and positrons are produced by the relic particles, or by some astrophysical sources. To distinguish between the two possibilities, one can compare the electron population in the local neighborhood with that in the dwarf spheroidal galaxies, which are not expected to host as many pulsars and other astrophysical sources. This can be accomplished using the X-ray observations of the dwarf spheroidal galaxies. Assuming the Fermi signal comes from dark matter and using the inferred dark matter profile of the Draco dwarf spheroidal galaxy, we calculate the spectrum of X-rays produced by electrons via inverse Compton scattering. The next generation of X-ray telescopes may be able to detect such a signal.

## I. INTRODUCTION

The nature of cosmological dark matter remains a tantalizing puzzle [1]. If dark matter is made up of weakly interacting massive particles (WIMP), their annihilation products may be observed and used for identification of the dark-matter particles. PAMELA [2], ATIC [3], PPB-BETS [4], and Fermi [5] have observed unexpected features in the electron and positron spectra at high energies. The high-energy electrons and positrons could come from the annihilations of dark matter particles [6–11], but they could also be produced by astrophysical sources, such as pulsars, supernova remnants and Gamma-Ray Bursts (GRBs) [12–16]. Theoretical models of dark matter can accommodate a wide range of parameters (see, for example, Refs. [13, 17, 18]). The astrophysical models of particle acceleration by pulsars are also uncertain, and they can account for the observed signal as well. To distinguish between the two possibilities, it would be desirable to compare the electron and positron populations in the local neighborhood with that in some other parts of the galaxy, which are known to be devoid of pulsars and other potential astrophysical sources of high-energy particles. Dwarf spheroidal galaxies present such an opportunity, provided that one can infer the electron-positron spectra from X-rays.

The X-ray observations of dwarf spheroidal galaxies have recently been used in a dedicated search for *decaying* dark matter in the form of sterile neutrinos [19, 20]. Sterile neutrinos are expected to undergo a two-body decay, producing a narrow line in the X-ray spectrum (for a recent review, see, e.g., Ref. [21]). Detection of WIMP, which are much heavier and which annihilate rather than decay, presents a very different challenge. For a number of WIMP models, the X-ray signals would be too faint to observe in the foreseeable future, but the same models would predict the flux of high-energy electrons and positrons well below the levels observed by PAMELA, ATIC, PPB-BETS, and Fermi. A Breit-Wigner resonance [9] or long-range interactions [6, 22] could increase the dark matter annihilation cross section, but it is difficult to reconcile Sommerfeld enhancement with the primordial relic abundance of WIMP [23]. One does expect a boost factor from the small scale structure of dark matter, but the required values are well in excess of one's expectations based on numerical N-body simulations.

In the absence of a compelling theoretical framework, we will not try to relate our predictions to any specific model of dark matter, but we will focus on a model-independent determination of whether the high-energy electrons originate from dark matter (which is abundant in both the local neighborhood and a dwarf spheroidal galaxy), or from some astrophysical source candidates (whose population in a dwarf spheroidal galaxy is suppressed).

---

\*Electronic address: acalvez@ucla.edu

## II. X-RAY SPECTRA

Let us consider the spectrum of cosmic microwave background (CMB) photons, up-scattered to the X-ray band by the inverse Compton scattering (ICS) of electrons and positrons produced by the annihilation of dark-matter particles in a dwarf spheroidal galaxy. For any self annihilating dark matter candidate, we define the number density per unit time and energy of a certain species  $i$  in the final state of the reaction as

$$Q_i(\vec{r}, E) = \langle \sigma v \rangle_0 \frac{\rho_\chi^2(\vec{r})}{2m_\chi^2} N_i(E), \quad (1)$$

where  $N_i(E)$  describes the differential number of particle of species  $i$  produced per annihilation, as a function of energy; this and the annihilation rate at zero temperature  $\langle \sigma v \rangle_0$  are the only parameters in Eq. (1) that are sensitive to the dark matter model. In reality, however,  $\langle \sigma v \rangle_0$  is strongly constrained by dark-matter abundance inferred from WMAP data [24]. The remaining parameters are the mass of the dark matter particle  $m_\chi$ , and the halo density profile of dark matter as a function of the radius  $\rho_\chi(\vec{r})$ , which we will take to be the Navarro, Frenk and White (NFW) profile [25].

To calculate the X-ray spectrum generated by the IC scattering of electrons and positrons off of CMB photons, we consider the production of electrons and positrons and their propagation in the interstellar medium until the point where they interact. In principle, the process could be simulated using a numerical program, such as GALPROP, but little is known about the properties of the interstellar medium surrounding dwarf spheroidal galaxies. We feel that, given the uncertainties, using an analytical model of diffusion and energy loss is adequate, while the effects of various assumptions are more evident in such analytical calculation. To determine the differential electron density we will follow Refs. [26–28] and model the diffusion and energy loss with the following transport equation:

$$\frac{\partial}{\partial t} \frac{dn_e}{dE} = \nabla \left[ D(E, \vec{r}) \nabla \frac{dn_e}{dE} \right] + \frac{\partial}{\partial E} \left[ b(E, \vec{r}) \frac{dn_e}{dE} \right] + Q_e(E, \vec{r}), \quad (2)$$

where  $D(E, \vec{r})$  is the diffusion coefficient,  $b(E, \vec{r})$  is the energy loss term, and  $\frac{dn_e}{dE}$  is the sum of the differential electron and positron densities. Under the simplifying assumptions that the system has reached equilibrium, and that the diffusion and the energy loss terms are spatially homogeneous, Eq. (2) becomes:

$$D(E) \nabla^2 \frac{dn_e}{dE} + \frac{\partial}{\partial E} \left[ b(E) \frac{dn_e}{dE} \right] + Q_e(E, \vec{r}) = 0. \quad (3)$$

We will assume a diffusion term of the form [26, 29, 30]:

$$D(E) = \frac{d_B^{2/3}}{B_\mu^{1/3}} D_0 \left( \frac{E}{1 \text{ GeV}} \right)^\gamma, \quad (4)$$

where  $d_B$  is the minimum scale of uniformity of the magnetic field,  $B_\mu$  is the size of the magnetic field in  $\mu\text{G}$  and  $D_0$  is a constant.

A slightly different model was considered in Ref. [31] to study the energy spectrum of synchrotron radiation in the Milky Way. Although the study assumed a departure from equilibrium, and a constant diffusion coefficient, it found an electron spectrum similar to our results.

Based on the analysis of cosmic ray fluxes in the Milky Way Ref. [32] found  $0 \leq \gamma \leq 1$  with a preferred value of  $\gamma = 0.7$ . The value of  $d_B^{2/3} D_0$  is not well known. In the same reference, a median value of  $D_0 = 1.1 \times 10^{27} \text{ cm}^2 \text{ s}^{-1}$  was used. However, this parameter depends on the magnitude and size of magnetic field inhomogeneities, which are unknown for such systems as dwarf spheroidal galaxies. Our choice of parameter will be discussed further in Section III B.

The energy loss term is [26, 28]

$$\begin{aligned} b(E) &= b_{IC}(E) + b_{syn}(E, B) + b_{coul}(E) + b_{brem}(E) \\ b(E) &= b_{IC}^0 \left( \frac{E}{1 \text{ GeV}} \right)^2 \\ &+ b_{syn}^0 \left( \frac{B}{1 \mu\text{G}} \right) \left( \frac{E}{1 \text{ GeV}} \right)^2 \\ &+ b_{coul}^0 n \left( 1 + \frac{1}{75} \log \left( \frac{\gamma_e}{n} \right) \right) \\ &+ b_{brem}^0 n \left( \log \left( \frac{\gamma_e}{n} \right) + 0.36 \right) \left( \frac{E}{1 \text{ GeV}} \right), \end{aligned}$$

where  $b_{IC}^0 = 0.25 \times 10^{-16} \text{ GeV s}^{-1}$ ,  $b_{syn}^0 = 0.0254 \times 10^{-16} \text{ GeV s}^{-1}$ ,  $b_{coul}^0 = 6.13 \times 10^{-16} \text{ GeV s}^{-1}$  and  $b_{brem}^0 = 1.51 \times 10^{-16} \text{ GeV s}^{-1}$ ;  $n$  defines the electron thermal density and is taken to be  $n = 10^{-6} \text{ cm}^{-3}$ , while  $\gamma_e$  is the usual relativistic  $\gamma$ -factor of the electron.

Eq. (3) can be solved exactly [26]. The solution takes the form:

$$\frac{dn_e}{dE}(E, \vec{r}) = \frac{1}{b(E)} \int_E^{M_\chi} dE' G(r, \Delta v) Q_e(E', \vec{r}), \quad (5)$$

where

$$\begin{aligned} G(r, \Delta v) &= \frac{1}{\sqrt{4\pi\Delta v}} \sum_{n=-\infty}^{\infty} (-1)^n \int_0^{r_h} dr' \frac{r'}{r_n} \frac{\rho_\chi^2(r')}{\rho_\chi^2(r)} \\ &\times \left[ \exp \left( -\frac{(r' - r_n)^2}{4\Delta v} \right) - \exp \left( -\frac{(r' + r_n)^2}{4\Delta v} \right) \right]. \end{aligned} \quad (6)$$

Here  $r_n = (-1)^n r + 2nr_h$ , and  $r_h$  is the diffusion radius. We will take our diffusion radius to be twice the visible radius. This decision is well motivated based on the results presented in Section III B. Finally we will define  $\Delta v = v(E) - v(E')$  with:

$$\begin{aligned} v(\chi) &= \int_{\chi_{\min}}^{\chi} dy D(y) \\ \chi(E) &= \int_E^{E_{\max}} \frac{dE'}{b(E')}. \end{aligned} \quad (7)$$

For the relevant parameter values for this problem, Eq. (6) is safely convergent after 10 iterations. In the case where the diffusion coefficient is set to zero, the first term on the left hand side of Eq. (3) vanishes, and an explicit solutions can easily be obtained by direct integration:

$$\left(\frac{dn_e}{dE}\right)_{\text{ND}} = \frac{1}{b(E)} \int_E^{m_\times} dE' Q_e(E', r). \quad (8)$$

$$\frac{dN_p}{dt d\epsilon_u}(\epsilon_u, \epsilon, \gamma_e) = \frac{2\pi r_0^2 c n(\epsilon)}{\gamma_e^2 \epsilon} \left[ 2q \ln q + (1+2q)(1-q) + \frac{\Gamma^2 q^2}{2(1+\Gamma q)}(1-q) \right] \quad (9)$$

where

$$\Gamma = \frac{4\epsilon\gamma_e}{m_e c^2}, \quad q = \frac{E_u}{\Gamma(1-E_u)}, \quad E_u = \frac{\epsilon_u}{\gamma_e m_e c^2},$$

$\epsilon_u$  is the energy of the up-scattered photon,  $n(\epsilon)$  is the black-body spectrum, and  $r_0$  is the classical electron radius. Finally, one obtains the overall photon spectrum:

$$\frac{dN_{X\text{-ray}}}{dt d\epsilon_u}(\epsilon_u) = \int dE d\epsilon dV \frac{dN_p}{dt d\epsilon_u} \frac{dn_e}{dE}. \quad (10)$$

The volume integral is performed over the entire halo of the observed dwarf spheroidal, and the two integrals over the incoming electron and photon energies are performed over the kinematically allowed range [33]. The flux near the earth can then easily be calculated:

$$\mathcal{F}(\epsilon_u) = \frac{1}{4\pi D_D^2} \frac{dN_{X\text{-ray}}}{dt d\epsilon_u}(\epsilon_u),$$

where  $D_D$  represents the distance between the earth and the dwarf spheroidal galaxy.

### III. APPLICATION

#### A. Source function from Pamela and Fermi

One would like to deduce a model independent source function,  $Q(E, \vec{r})$ , for dark matter annihilations based on the Pamela and Fermi results. If one assumes that the function doesn't change with time, then from Eq. (1) one can write:

$$Q(E, \vec{r}) = q(E) \rho_\chi^2(\vec{r}), \quad (11)$$

where  $q(E)$  contains all model dependant terms, including the boost factors.

If we consider the flux per unit energy caused by an infinitesimal element of  $Q$  and assume spherical symmetry we find,

$$\frac{d\mathcal{F}}{dE} = q(E) \rho_\chi^2(r) dr \quad (12)$$

These relativistic electrons have enough energy to up-scatter CMB photons to the X-ray band through inverse Compton scattering. In the Klein-Nishina limit where in the rest frame of the electron the energy of the photon  $\epsilon \gg m_e c^2$ , the energy spectrum of the up-scattered photon is [33]:

It seems reasonable to integrate this out to the typical propagation length of the electrons given by [26]

$$l_{\text{prop}} \approx \sqrt{\frac{D(E)E}{b(E)}}, \quad (13)$$

where the functions  $D(E)$  and  $b(E)$  were defined previously. We take  $D_0 = 1.1 \times 10^{27} \text{cm}^2 \text{s}^{-1}$ ,  $\gamma = 0.7$  and use IC scattering as the dominant part of  $b(E)$ . Since  $l_{\text{prop}}$  is only a few kpc's we take  $\rho_\chi(r)$  as roughly constant at  $0.35 \text{GeVcm}^{-3}$  and compare the total flux to those measured by Pamela and Fermi to get

$$q(E) = \beta \left( \frac{E}{1 \text{GeV}} \right)^{-a} \quad (14)$$

Where  $\beta \sim 6 \times 10^{-26} \text{GeV}^{-3} \text{cm}^3 \text{s}^{-1}$  and  $a \sim 1.88$ .

#### B. Choice of diffusion constant

Very little is known about the interstellar medium and magnetic fields in dwarf spheroidal galaxies. The dynamo mechanism driven by differential rotation and the wind and cosmic rays produced in supernovae are almost certainly not operational in a dwarf spheroidal galaxy [34, 35]. While it is possible that the dwarf spheroidals could create their own galactic wind due to the energy output by stars [36], they should be strongly affected by ram pressure and stripping due to the wind of the mother galaxy [37]. It is probably unlikely that appreciable magnetic fields could build up in dwarf spheroidals, and so the effects of diffusion should not be very important. However, for the purpose of completeness in comparing our results with the others we include diffusion in our analysis. Since the dynamo action is almost certainly not scalable from the mother galaxy to dwarf galaxies, the value of  $D_0$  can differ significantly from what one obtains using the scaling arguments. If one assumes that the spectrum of fluctuations of the magnetic field follows a Kolmogorov spectrum, one can show

that the diffusion constant must be given by Eq. (4). Since very little is known about the magnetic field structure of dwarf spheroidal galaxies we look at a range of possibilities from  $10^{26}\text{cm}^2\text{s}^{-1}$  to  $10^{27}\text{cm}^2\text{s}^{-1}$ . We also vary the magnetic field from  $0.1 - 1.0\ \mu\text{G}$ . If the magnetic field were much smaller than this or  $d_B^{2/3}D_0$  any larger then virtually no X-ray signal would be seen.

The choice of  $D_0$  strongly affects our attenuation length. By setting the attenuation length to the diffusion radius we can get a lower energy cutoff for our integrals. Energies below this would not interact within the dwarf spheroidal galaxy and can be ignored. If this energy is lower than the lowest energy for which an excess of electrons/positrons was seen (roughly 10 GeV), then we set the cutoff at 10 GeV.

Attenuation lengths are best estimated by  $\sqrt{\Delta v}$ . This is because the time it takes for the electrons and positrons to lose an energy  $\Delta E = E' - E$  between production and interaction is given by

$$\tau_{\text{loss}} = \int_{E'}^E \frac{d\varepsilon}{b(\varepsilon)}.$$

Therefore Eq. (7) describes the characteristic distance traveled by the electrons and positrons during that time. Figures 1(b)-1(a) present how  $\sqrt{\Delta v}$  varies for a typical set of parameters.

#### IV. ANALYTICAL APPROXIMATIONS

When the energy loss happens on scales much lower than the diffusion radius, one can ignore the term with  $D_0$ . In this simple case the diffusion equation can be solved analytically, and can be used to study the general behavior of the electron population.

We assume IC scattering is the dominant energy loss process. The term in brackets in Eq. (9), from the Klein-Nishina cross section, is very close to unity when  $\epsilon_u$  is around a few keV so we set it to 1 (i.e. in the Thompson limit). This conceals the dependence of the spectrum on  $\epsilon_u$ , but suggests that around a few keV the spectrum should be slowly varying with respect to  $\epsilon_u$ .

From Eq. (8) one obtains:

$$\left(\frac{dn_e}{dE}\right)_{\text{ND}} = \beta \frac{\rho_\chi^2(r)}{b_{\text{IC}}^0 E^2} \int_E^{m_\chi} dE' E'^{-1.88}. \quad (15)$$

Using the NFW profile:

$$\rho_\chi(r) = \frac{\rho_c}{\left(\frac{r}{R_S}\right)\left(1 + \frac{r}{R_S}\right)^2}, \quad (16)$$

and the equations from the previous sections we get

$$\frac{dN_{X\text{-ray}}}{dt d\epsilon_u}(\epsilon_u) = \frac{cr_0^2(m_e c)^2(kT)^2\beta R_S^3\rho_c^2}{648(\hbar c)^3 b_0 D_0^2} \left[1 - \left(1 + \frac{R_{\text{max}}}{R_S}\right)^{-3}\right] (5.3E_{\text{min}}^{-3.88} + 1.55M_\chi^{-3.88} - 6.8M_\chi^{-0.88}E_{\text{min}}^{-3}) \quad (17)$$

This equation is essentially an upper limit on the spectrum and should approach the correct answer at low  $\epsilon_u$ . This result shows the strong dependence of the spectrum on  $E_{\text{min}}$  and justifies our careful treatment of approximating it.

#### A. Results

In Figure 2(a) through Figure 2(d) we present the results of our analysis in the absence of diffusion (labeled  $ND$  for “no diffusion” in the legend), and for values of  $D_0$  between  $10^{26}\text{cm}^2\text{s}^{-1}$  and  $10^{27}\text{cm}^2\text{s}^{-1}$ . For the cases where diffusion is present, we plot the differential number of photons for  $\gamma = 0.3$ , and  $\gamma = 0.7$ . The magnetic field’s magnitude is varied between  $B = 1\ \mu\text{G}$  and  $B = 100\ \text{nG}$ . Again, as mentioned in section III B because of the absence on any interstellar gas in dwarf spheroidals, we believe that the electron transport should proceed without diffusion. We include plots of the photon spectrum assuming non-diffusionless transport for comparison purposes only.

The fact that the non-diffusion case dominates for some range of parameters can be understood by looking at the Green’s function of the transport equation. Comparing Eq. (5) and (8), we see that all the information about the diffusive process is encoded inside the Green’s function. We plot Eq. (6) in Figure 3.

In the region where  $0.2 \lesssim \left(\frac{\Delta v}{1\ \text{kpc}^2}\right) < 1$ , there is a significant enhancement in the value of the Green’s function. Physically we can understand that result as follows. When the effects of diffusion are very small, the Green’s function is equal to  $G = 1$ , and the results are equivalent to the no-diffusion case, as seen in Figure 2(b). When the diffusion constant is very large, the particles leave the system before they have a chance to interact yielding  $G < 1$ , and decreasing the overall final ICS photon flux as in Figure 2(d) and 2(c). In the intermediate case, diffusion effectively traps the electrons and the positrons in the system, giving them more time to interact with the CMB yielding  $G > 1$ , and effectively boosting the final photon flux as in Figure 2(a).

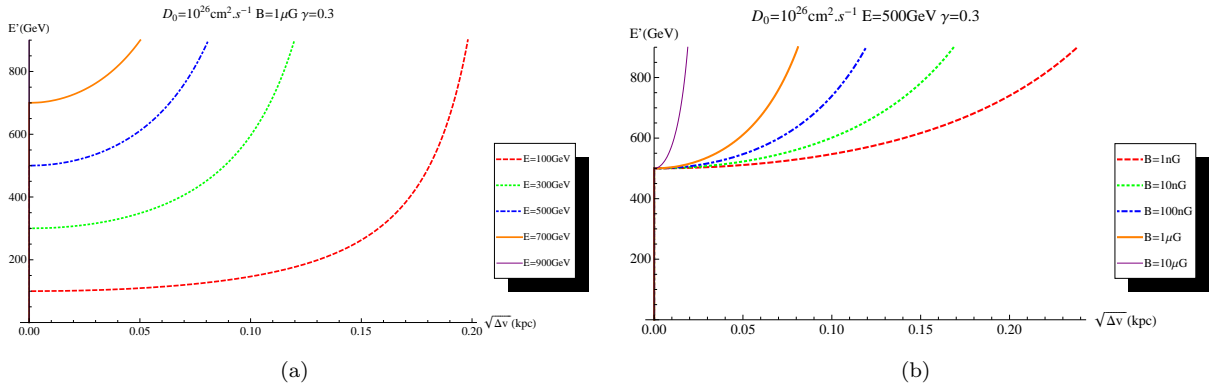


FIG. 1: The average distance traveled by an electron/positron between its emission with energy  $E'$ , and its interaction at energy  $E$  for two sets of parameters: (a)  $D_0 = 10^{26} \text{ cm}^2 \text{ s}^{-1}$ ,  $B = 1 \mu\text{G}$  and  $\gamma = 0.3$ , and (b)  $D_0 = 10^{26} \text{ cm}^2 \text{ s}^{-1}$ ,  $E = 500 \text{ GeV}$  and  $\gamma = 0.3$ .

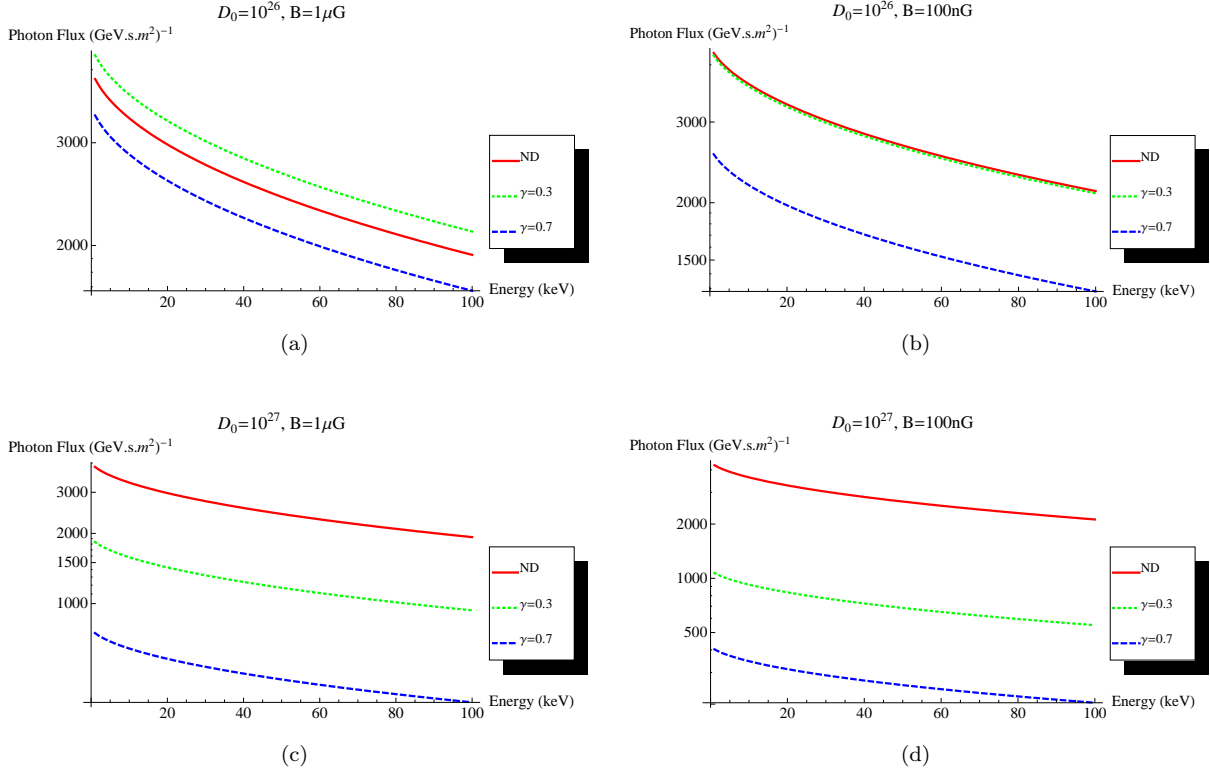


FIG. 2: Photon spectra in the absence of diffusion (solid red line), for  $\gamma = 0.3$  (green, dotted line), and for  $\gamma = 0.7$  (blue, dashed line). Fig. 2(a): diffusion constant  $D_0 = 10^{26} \text{ cm}^2 \text{ s}^{-1}$ , magnetic field  $B = 1 \mu\text{G}$ . Fig. 2(b):  $D_0 = 10^{26} \text{ cm}^2 \text{ s}^{-1}$ ,  $B = 100 \text{ nG}$ . Fig. 2(c):  $D_0 = 10^{26} \text{ cm}^2 \text{ s}^{-1}$ ,  $B = 1 \mu\text{G}$ . Fig. 2(d):  $D_0 = 10^{27} \text{ cm}^2 \text{ s}^{-1}$ ,  $B = 100 \text{ nG}$ .

Our predicted signal in the hard X-ray band cannot be detected by the non-imaging detectors currently in orbit such as the *Suzaku* Hard X-ray Detector, because it is overwhelmed by cosmic X-ray background photons in the spectra extracted in these large beams. However it may be measurable in observations of nearby, high dark-

matter-density dwarf spheroidals using the next generation of hard X-ray imaging telescopes, e.g. *NuStar*. Such a result would allow us to narrow the number of candidates responsible for the large population of high energy electron and positrons in the interstellar medium.

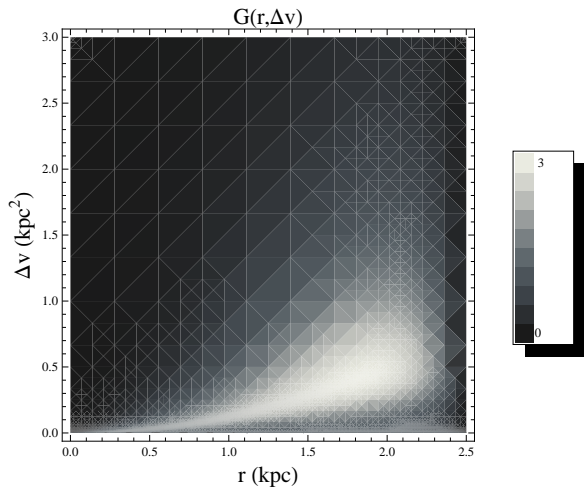


FIG. 3: Representation of the Green's function in Eq. (6) for  $\gamma = 0.3$  and  $D_0 = 10^{26} \text{cm}^2 \text{s}^{-1}$ .

## V. CONCLUSION

Future observations of dwarf spheroidal galaxies with the next generation X-ray telescopes may be able to probe the origin of high-energy electrons and positrons observed by Fermi and PAMELA. The litmus test for

dark matter annihilations as the possible origin of these signals comes from comparing the high-energy particle fluxes in a dwarf spheroidal galaxy and in the local neighborhood of the Milky Way disk. Dark matter dominated systems, such as dwarf spheroidal galaxies, should generate a predictable flux of the dark-matter annihilations products, subject to mass model uncertainties. At the same time, most of the astrophysical sources capable of producing high-energy particles in the sun's neighborhood are absent in dwarf spheroidal galaxies, which have very few stars and very little gas, as compared with their dark matter content. The high-energy electrons and positrons produced in dwarf spheroidals can generate X-rays by up-scattering CMB photons to the X-ray energy band. While the predicted fluxes are below the sensitivity of current X-ray telescopes, they should be observable by the next generation of X-ray instruments.

## Acknowledgments

A.K. thanks P. Biermann for helpful comments. This work was supported in part by DOE grant DE-FG03-91ER40662 and by the NASA ATRP grant NNX08AL48G. MF acknowledges support from the EU Marie Curie Network UniverseNet (HPRN-CT-2006-035863).

- 
- [1] G. Bertone, D. Hooper, and J. Silk, *Phys. Rept.* **405**, 279 (2005), hep-ph/0404175.
  - [2] O. Adriani et al. (PAMELA), *Nature* **458**, 607 (2009), 0810.4995.
  - [3] J. Chang et al., *Nature* **456**, 362 (2008).
  - [4] S. Torii et al. (PPB-BETS) (2008), 0809.0760.
  - [5] A. A. Abdo et al. (The Fermi LAT) (2009), 0905.0025.
  - [6] N. Arkani-Hamed, D. P. Finkbeiner, T. R. Slatyer, and N. Weiner, *Phys. Rev.* **D79**, 015014 (2009), 0810.0713.
  - [7] C.-R. Chen, F. Takahashi, and T. T. Yanagida, *Phys. Lett.* **B673**, 255 (2009), 0811.0477.
  - [8] P. J. Fox and E. Poppitz, *Phys. Rev.* **D79**, 083528 (2009), 0811.0399.
  - [9] M. Ibe, H. Murayama, and T. T. Yanagida, *Phys. Rev.* **D79**, 095009 (2009), 0812.0072.
  - [10] M. Ibe, Y. Nakayama, H. Murayama, and T. T. Yanagida, *JHEP* **04**, 087 (2009), 0902.2914.
  - [11] S. Shirai, F. Takahashi, and T. T. Yanagida (2009), 0905.3235.
  - [12] K. Ioka (2009), 0812.4851v3.
  - [13] S. Profumo (2008), 0812.4457.
  - [14] A. Calvez and A. Kusenko (2010), 1003.0045.
  - [15] L. Stawarz, V. Petrosian, and R. D. Blandford, *Astrophys. J.* **710**, 236 (2010), 0908.1094.
  - [16] H. Yuksel, M. D. Kistler, and T. Stanev, *Phys. Rev. Lett.* **103**, 051101 (2009), 0810.2784.
  - [17] M. Cirelli, M. Kadastik, M. Raidal, and A. Strumia, *Nucl. Phys.* **B813**, 1 (2009), 0809.2409.
  - [18] D. Grasso et al. (FERMI-LAT) (2009), 0905.0636.
  - [19] M. Loewenstein and A. Kusenko (2009), 0912.0552.
  - [20] M. Loewenstein, A. Kusenko, and P. L. Biermann, *Astrophys. J.* **700**, 426 (2009), 0812.2710.
  - [21] A. Kusenko, *Phys. Rept.* **481**, 1 (2009), 0906.2968.
  - [22] M. Lattanzi and J. I. Silk, *Phys. Rev.* **D79**, 083523 (2009), 0812.0360.
  - [23] J. L. Feng, M. Kaplinghat, and H.-B. Yu (2009), 0911.0422.
  - [24] G. Hinshaw et al. (WMAP), *Astrophys. J. Suppl.* **180**, 225 (2009), 0803.0732.
  - [25] J. F. Navarro, C. S. Frenk, and S. D. M. White, *Astrophys. J.* **462**, 563 (1996), astro-ph/9508025.
  - [26] S. Colafrancesco, S. Profumo, and P. Ullio, *Astron. Astrophys.* **455**, 21 (2006), astro-ph/0507575.
  - [27] S. Colafrancesco, S. Profumo, and P. Ullio, *Phys. Rev.* **D75**, 023513 (2007), astro-ph/0607073.
  - [28] T. E. Jeltema and S. Profumo (2008), 0805.1054.
  - [29] P. Blasi and S. Colafrancesco, *Astropart. Phys.* **122**, 169 (1999), astro-ph/9905122.
  - [30] S. Colafrancesco and P. Blasi, *Astropart. Phys.* **9**, 227 (1998), astro-ph/9804262.
  - [31] S. I. Syrovat-Skii, *Soviet Astronomy* **3**, 22 (1959).
  - [32] F. Donato, N. Fornengo, D. Maurin, and P. Salati, *Phys. Rev.* **D69**, 063501 (2004), astro-ph/0306207.
  - [33] G. R. Blumenthal and R. J. Gould, *Rev. Mod. Phys.* **42**, 237 (1970).
  - [34] M. Hanasz, G. Kowal, K. Otmianowska-Mazur, and H. Lesch, *Astrophys. J.* **605**, L33 (2004), arXiv:astro-ph/0402662.

- [35] E. N. Parker, *Astrophys. J.* **401**, 137 (1992).
- [36] R. Barvainis, G. McIntosh, and C. R. Predmore, *Nature (London)* **329**, 613 (1987).
- [37] J. E. Everett, E. G. Zweibel, R. A. Benjamin, D. Mc-  
Cammon, L. Rocks, and I. J. S. Gallagher, *Astrophys. J.* **674**, 258 (2008), 0710.3712.